Science Advances
AAAS

advances.sciencemag.org/cgi/content/full/4/8/eaat0127/DC1

Supplementary Materials for

Photothermal trap utilizing solar illumination for ice mitigation

Susmita Dash, Jolet de Ruiter, Kripa K. Varanasi*

*Corresponding author. Email: varanasi@mit.edu

Published 31 August 2018, *Sci. Adv.* **4**, eaat0127 (2018)
DOI: 10.1126/sciadv.aat0127

The PDF file includes:

Other Supplementary Material for this manuscript includes the following:

(available at advances.sciencemag.org/cgi/content/full/4/8/eaat0127/DC1)

Section S1. Absorptivity of materials

The absorptivity of the different surfaces is measured using a UV/Vis spectrophotometer, and shown in fig. S1. The cermet (MT1300 mirotherm®, Alanod GmbH) coating has outstanding absorptivity with respect to uncoated aluminum. The absorptivity is weighted for the spectral power distribution of a halogen source (color temperature: 3250 K) with IR-filter, over the wavelength range 400-800nm. This yields an average absorptivity of 96% for cermet-coated aluminum *versus* 27% for uncoated aluminum – to be used as parameter values in the numerical model. The presence of a hydrophobic Teflon layer has almost no effect on average absorptivity. For the full sunlight spectrum, the absorptivity of the cermet coating has been specified by the supplier as 95 ± 1%, so this value is similar for both laboratory and outdoor conditions.

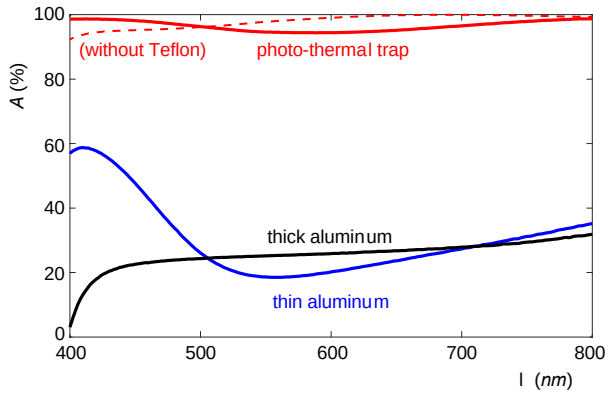

Fig. S1. Sample absorptivity. Absorptivity (%) as a function of wavelength (400-800 nm) for the photo-thermal trap coated with cermet (red) *versus* uncoated aluminum (thin and thick sample: blue and black, respectively). All surfaces are coated with Teflon for hydrophobicity, except for the photo-thermal trap reference case indicated by the red dashed line.

The coating remained intact during the entire duration of our study, which include repeated experiments with single droplets and frost formation (in both laboratory and outdoor experiments) on a single substrate, and over a period of one year. We did not perceive any variation in absorptivity, photothermal trap efficiency, or wettability.

Section S2. Estimation of temporal temperature rise of the substrate due to illumination

In the absence of forced convection, flow above the surface is solely buoyancy driven, and can be modeled as convection over a hot plate (in this case, the surface is heated by the absorbed

incidence). The magnitude of *h* thus depends on the relative difference in surface and ambient temperature, and is given by $h = 0.59Ra^{1/4}(k_{air}/L_c)$, where Ra is the Rayleigh number; $Ra = g\beta(T - T_{amb})\left[{L_c}^3/(\gamma\alpha)\right]$ where β is the thermal expansion coefficient, L_c is the characteristic length scale of the substrate, and k_{air}, γ and α are the thermal conductivity, kinematic viscosity and thermal diffusivity of air, respectively. Below the insulation layer, the heat transfer will be influenced to some extent by the nature of the base substrate (note its influence is minimized due to the presence of insulation). Here we assume that the heat transfer to the backside of the insulation is dictated by buoyant convection in the air. The heat transfer coefficient (h_1) at insulation-air side is lower than *h* on the topside of the substrate and ice due to lower temperature difference with respect to the ambient. Note that the thin metal layer at the top of the photo-thermal trap is considered at uniform temperature since the associated Biot number, $Bi = (h\delta)/k < 0.1$. Here, δ and k are the thickness and thermal conductivity of the metal layer, respectively.

The governing equations, Eq. (1) through (3) in the manuscript, are solved using finite volume method using a forward difference scheme in space and time to obtain the temporal substrate temperature. A schematic of the control volume and discretization in the thermal spreader, ice and insulation layers is shown in fig. S2. The temperature of the substrate, ice and insulation are initially in equilibrium with the ambient. The boundary conditions are given by $T_{ice}|_{x_{ice}=0} = T$ and $T_{ins}|_{x_{ins}=0} = T$ at the plane of contact of ice ($x_{ice} = 0$) and insulation ($x_{ins} = 0$) with the metal layer, respectively. The other boundary condition is that the heat conducted through ice, or insulation, is equal to the heat convected at the ice-air, or insulation-air/base substrate, interface. The converged values of temperature at each time step are used to determine the corresponding thermophysical properties of air and heat transfer coefficients. The temperature profile of the heat spreader is then curve fitted using an exponential curve in the form of $\Delta T = \Delta T_{eq}\left(1 - e^{-t/\tau}\right)$ to determine the steady state temperature rise, ΔT_{eq} and thermal time constant, τ.

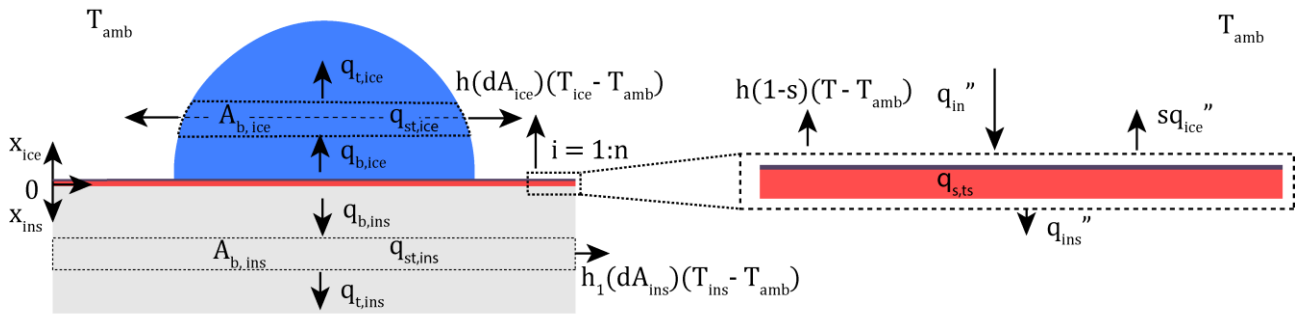

Fig. S2. Control volume approach to determine the transient temperature evolution of the metal spreader upon illumination. Control volumes are taken in the ice and insulation to find their respective temperature gradients, while the metal spreader is at homogeneous temperature.

Section S3. Freezing and melting movies

Movie S1 shows the controlled freezing of a water droplet supercooled to −17 °C, leading to two-stage phase-change, *i.e.* recalescence and freezing. The video corresponds to Fig. 2a in the main text. Subsequently, movie S2 shows the melting behavior of an illuminated droplet on the photo-thermal trap. The video corresponds to the snapshots in Fig. 2b in the main text.

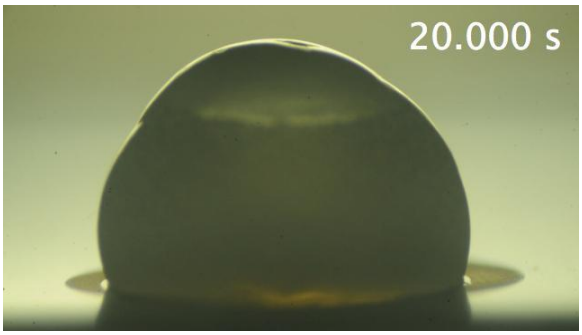

Movie S1. Droplet freezing. Freezing of a 40-μl droplet on the photo-thermal trap, supercooled to −17 °C at an ambient temperature of approximately −20 °C. Time sequence is shown from 10 seconds before to 50 seconds after recalescence. The video is shown in real-time (recorded at 24 Hz and compressed to 8 Hz).

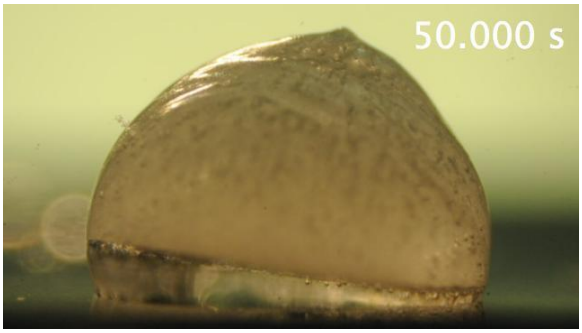

Movie S2. Droplet melting. Melting of a 40-μl (frozen) droplet on the photo-thermal trap, at an ambient temperature of -25 °C and 1.8 kW/m^2 illumination starting at $t = 0$. Time sequence is shown from 5 seconds before to 120 seconds after start of illumination. The video is shown in real-time (recorded at 24 Hz and compressed to 8 Hz).

Section S4. Droplet sliding upon illumination

Movie S3 shows the sliding of a droplet off an inclined photo-thermal trap due to the melt layer formed upon illumination. The video corresponds to the experiment shown in Fig. 4a in the main text.

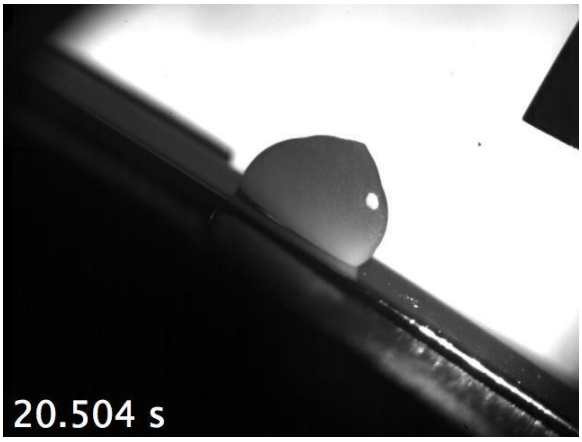

Movie S3. Droplet sliding on melt layer. The substrate is inclined at 30° and the ambient temperature is kept at $T_{amb} = -15$ °C. At $t = 0$ the photo-thermal trap with 40-μl frozen drop is illuminated with 1.8 kW/m^2 power density. (Illumination at the lower side of the incline explains the increasing brightness when the drop starts moving). Sliding starts promptly when a thin liquid film is present, here 19.8 seconds after illumination. Time sequence is shown from 19.6 to 21.0 seconds after start of illumination. The video is recorded at 125 Hz and shown with 10× delay.

Section S5. Demonstration experiment with forced convection

We performed a demonstration experiment at a higher heat transfer coefficient using an external flow. Cooled nitrogen is led into the experimental chamber, flowing parallel to the test surface, and positioned such that it flows directly over the surface. The ambient temperature is maintained around −7 °C. We illuminate a frozen droplet with 1.0 kW/m^2 power, and find that the equilibrium temperature rise is 7 °C, see fig. S3a. Although this is 5× lower than the stagnant-air case, the temperature rise is sufficient to melt the droplet under the current experimental conditions, as shown in fig. S3b. Melting starts 40 seconds after illumination, but then proceeds only very slowly since the surface temperature stabilized exactly around 0 °C. Over the duration of 15 minutes, there is evaporation-induced reduction in drop volume (fig. S3b). Since the surface reaches exactly zero degree temperature, the experiment was performed at critical conditions, and the numerical prediction (presented in Figure 3c of the main text) can be used to estimate the heat transfer coefficient. The observed characteristic time scale in the experiment, 20 seconds, predicts a heat transfer coefficient of ~ 70 W/m^2/K. The corresponding temperature rise of 10 °C is in good agreement with the experimentally observed value (7 °C).

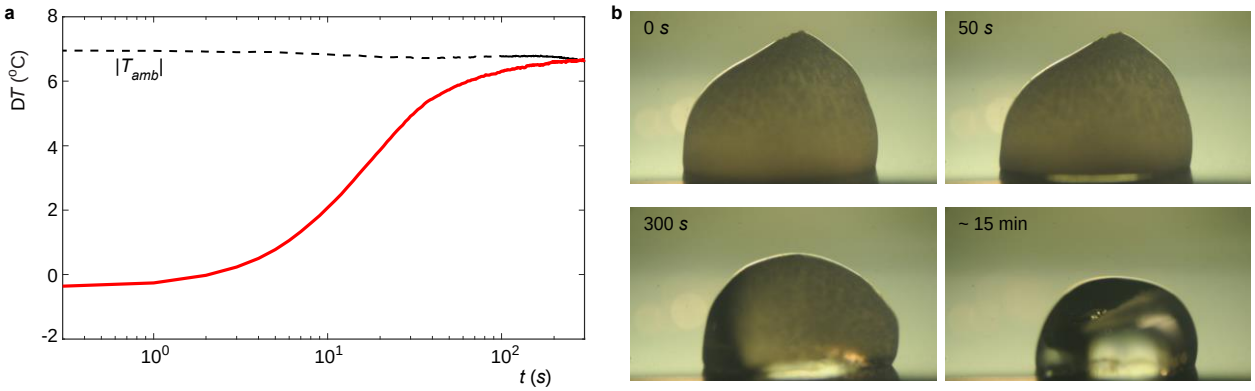

Fig. S3. Substrate under direct shear flow. a Heating curve (red) for 1 kW/m^2 illumination of the photo-thermal trap at ambient temperature of −7 °C (black dashed), and a shear flow leading to increased heat transfer coefficient h~70 W/m^2/K. **b** Snapshots show intermediate steps in the progression of melting on the photo-thermal trap.

Section S6. Melting of frost layer

Movie S4 shows the melting of a frost layer at −15 °C ambient temperature. The video corresponds to the experiment shown in Fig. 4b in the main text.

Movie S4. Melting of frost layer. At $t = 0$ the substrate is illuminated with 1.8 kW/m^2 power density, through the frost layer, at its right side outside the video frame. Melting proceeds from right to left in two stages: first the interfacial layer melts, followed by bulk melting that allows collection of most of the liquid by *de*-wetting, leaving only a few residual microdroplets on the surface. Ambient temperature is -15 °C. Time sequence is shown from 10 seconds before to 50 seconds after start of illumination. The video is shown in real-time (recorded at 24 Hz and compressed to 8 Hz). Full frame width is 15 mm.